Science of the Total Environment 957 (2024) 177353

Contents lists available at ScienceDirect

Science of the Total Environment

journal homepage: www.elsevier.com/locate/scitotenv

Influence of aging, morphology and particle size on the behavior of microplastics during magnetic seeded filtration

Steffen Kaiser [a], Ralf Kaegi [b,*], Frank Rhein [a]

[a] Karlsruhe Institute of Technology, Institute of Mechanical Process Engineering and Mechanics, Strasse am Forum 8, 76131 Karlsruhe, Germany
[b] Swiss Federal Institute of Aquatic Science and Technology, Ueberlandstrasse 133, 8600 Dübendorf, Switzerland

HIGHLIGHTS

- UV exposure resulted in polymer-specific reductions of the separation efficiencies.
- Mechanical aging lowered the separation efficiencies independent of polymer types
- Morphology and oxidative aging had only minor impacts on the separation efficiency.
- Changes in separation efficiency correlate with changes of microplastic surfaces.

GRAPHICAL ABSTRACT

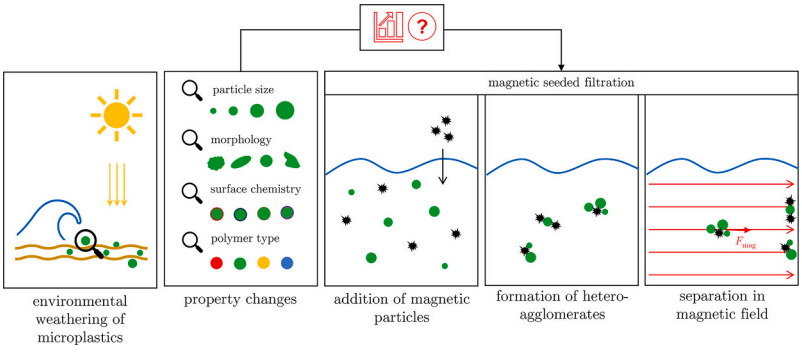

ARTICLE INFO

Editor: Damià Barceló

Keywords:
Microplastics
Magnetic separation
Aging
Surface properties
Hydrophobic interactions
Environmental samples

ABSTRACT

Magnetic seeded filtration (MSF) is a solid-liquid separation process based on the formation of hetero-agglomerates between target (non-magnetic) particles and added magnetic particles, followed by magnetic separation. Previous experimental studies reported high separation efficiencies for hydrophobic microplastic particles (MP) and focused mainly on the polymer type. This study investigates the influence of the particle size, morphology and aging on the separation efficiency of different polymer types.

Surface morphology and particle size only marginally affect the separation of particles larger than 30 μm. However, the agglomeration of particles in the lower micron range is increasingly dominated by repulsive electrostatic interactions. After oxidative treatment with Fenton's reagent, separation efficiencies for most MP remain between 55% and 96%. Exposure to UV light results in a significant decrease in separation efficiency, particularly for polystyrene, where the separation efficiency decreases from 86% to 9%. Mechanical aging, simulated by mixing MP in a sand matrix on a horizontal shaker, reduces the separation to below 50% for all polymer types.

Exposure to UV light causes surface oxidation, as evidenced by the formation of carbonyl peaks in the Fourier transformed infrared spectra. Mechanical treatment results in the deposition of small silica particles on the MP surface, as revealed by electron microscopy. Both mechanisms render the polymer surface more hydrophilic and reduce the tendency to form hetero-agglomerates with (hydrophobic) magnetic seed particles. MSF is a promising technique for MP separation but also offers the possibility to probe surface properties of (environmentally

* Corresponding author.
E-mail address: ralf.kaegi@eawag.ch (R. Kaegi).

https://doi.org/10.1016/j.scitotenv.2024.177353
Received 18 September 2024; Received in revised form 28 October 2024; Accepted 31 October 2024
Available online 16 November 2024

aged) MPs. This study demonstrates that environmental aging can significantly affect the behavior of MP and highlights the importance of environmental aging in MP fate studies.

Nomenclature

Most relevant abbreviations and labels

bl	blue
cryo	cryomilling / cryomilled
cut	cutting-milling / cutting-milled
Gf	Goodfellow
Mag	magnetic particles
Mech	mechanical aging
MP	microplastic particles
MSF	magnetic seeded filtration
ox	oxidative aging
PE	polyethylene
PET	polyethylene terephthalate
PMMA	polymethylmethacrylate
PP	polypropylene
pris	pristine
PS	polystyrene
PSD	particle size distribution
purch	purchased
PVC	polyvinyl chloride
SI	Supplementary Information
UV	UV aging
Vin	Vinnolit

Symbols

α	collision efficiency [−]
β	collision frequency [$m^{-3}s^{-1}$]
Φ	contact angle [°]
ρ	density [kg m^{-3}]
$\tilde{\nu}$	wave number [m^{-1}]
ϑ	temperature [°C]
A	separation efficiency [−]
a	loss ratio [−]
c_n	concentration [mol L^{-1}]
c_m	mass concentration [kg m^{-3}]
c_V	volume concentration [−]
f	frequency [s^{-1}]
I	ionic strength [mol m^{-3}]
m	mass [kg]
N	number [−]
n	rotation speed [s^{-1}]
P	power of irradiation [kg s^{-3}]
t	time [s]
V	volume [m^3]
x	diameter [m]
$x_{50,3}$	volume equivalent mean diameter [m]

1. Introduction

Since the start of the mass production of plastics in the 1950s, mankind has greatly benefited from these synthetic materials (Andrady and Neal, 2009; Geyer et al., 2017). Plastics combine many advantages, such as low density, high strength, flexibility in processing, long durability and cost-effective production (Andrady and Neal, 2009). In addition, the properties of plastics can be tailored during production offering applications in many different areas, including packaging and construction materials, transportation, cosmetics and medicine (Andrady and Neal, 2009; Geyer et al., 2017; Koltzenburg et al., 2014). As a consequence the amount of plastic produced annually has increased rapidly since the 1950s and is now approaching 400 million metric tonnes (*Plastics – the facts* 2023, n.d.).

The environmental persistence of plastic materials, combined with inefficient or inadequate waste management and poor recycling rates, results in an increasing amount of plastic pollution in the environment (Geyer et al., 2017; Liebmann, 2015; Jambeck et al., 2015). Environmental aging, dominated by the exposure to sunlight and the mechanical abrasion in for example river beds or on shorelines, lead to the fragmentation of larger plastic items (Liebmann, 2015; Jambeck et al., 2015; Andrady, 2017). This produces so-called microplastic particles (MP) defined as plastic particles with a diameter smaller than 5 mm (Thompson et al., 2004). In addition to the degradation of larger plastic items that enter the environment through littering, MP are also used directly in cosmetics, detergents and technical applications (Liebmann, 2015; Andrady, 2011; Birch et al., 2020).

These issues motivate the search for solid-liquid separation processes that are able to efficiently and selectively remove MP from suspensions. Established methods such as flotation, sedimentation and filtration often fail due to small differences between particle and matrix properties or due to small particle sizes and high dilutions (Zhang et al., 2021a). To overcome these challenges, magnetic seeded filtration (MSF) is investigated in current research. In this approach, (hydrophobic) magnetic particles (Mag) are added to the suspension and agglomerate with the MP. The agglomerates can then be separated in a magnetic field. Recent studies demonstrated high separation efficiencies for MP from aqueous suspensions using MSF on lab-scale (Rhein et al., 2019; Rhein et al., 2022; Grbic et al., 2019; Shi et al., 2022; Zhang et al., 2021b), whereas large-scale implementations are currently lacking. Although previous studies report high removal efficiencies for MP by MSF approaches, these studies mainly focused on pristine MP and leave questions regarding the impact of environmental aging on the separation efficiency largely unanswered. Furthermore, (Rhein et al., 2022) speculated that particle properties such as morphology and size additionally affect the separation efficiency of the MSF process.

This study, therefore, addressed the impact of different MP properties and weathering mechanisms on the separation efficiency during MSF. The investigated particle properties included particle size distribution (PSD), morphology and surface characteristics. Additionally, MP of different polymer types were aged by ultraviolet (UV) light exposure, oxidative treatment (cf. (Philipp et al., 2022)) and mechanical abrasion. To represent the majority of MP found in the environment, polyvinyllene (PE), polypropylene (PP), polystyrene (PS), polyethylene terephthalate (PET) and polyvinyl chloride (PVC) were investigated. This extensive and systematic variation of particle properties allowed for a better understanding of the behavior of MP during MSF, which to some extent, can be used to explain the behavior of MPs in environmental matrices.

2. Materials & methods

2.1. Magnetic seeded filtration theory

For an in-depth description of the theoretical background on hetero-

agglomeration and MSF we refer to our previous studies (Rhein et al., 2022; Rhein et al., 2023a). In brief, two particles must collide and "stick" upon collision to form an agglomerate. These effects are quantified by the collision frequency β and collision efficiency α, respectively. In this study, agglomeration is governed by fluid flow rather than by diffusion due to large particle diameters and β is both proportional to the mean shear rate and particle volume. α results from balancing all attractive and repulsive inter-particle interactions (van der Waals, electrostatic, hydrophobic) and is therefore dominated by surface properties of the particles and the chemistry of the surrounding media. After their formation, the hetero-agglomerates are separated on the basis of the magnetic force, which is primarily dependent on the gradient of the magnetic field strength, the magnetization and partial volume of the magnetic component. A previous study (Rhein et al., 2021) showed that separated agglomerates can be further processed to recycle both the magnetic component and – depending on the employed method – also the separated non-magnetic particles. This offers further possibilities to recycle the separated MP. Furthermore, in potential large-scale facilities, water dynamics would have to be managed in respective collision reactors to optimize the formation of hetero-agglomerates. Such aspects, however, were outside the scope of this work.

2.2. Analytical methods

2.2.1. Static laserlight scattering (SLS)

Particle size distributions were measured by SLS using a LS 13320 Laser Diffraction Particle Size Analyzer (Beckman Coulter Corporation, USA). Microplastic particles were dispersed in ethanol (EtOH) (EMSURE ethanol for analysis, Merck KGaA, Germany), which was more suitable compared to water and does not compromise the information content in context of the measured scattered light equivalent diameter. Stock suspensions were prepared and dispersed by shaking. After the background measurements, the suspensions were added to a cuvette until the signal intensity was sufficient for the measurement. Using the built-in stirrer, the measurements were conducted over $t = 30$ s. The measuring range was between $0.4\,\mu\text{m} \leq x \leq 2000\,\mu\text{m}$ and for evaluation the `Fraunhofer.rf780d` model was used at wavelength 780 nm.

2.2.2. Fourier transform infrared (FTIR) spectroscopy

Fourier transform infrared spectra of MP were recorded using a Cary 670-IR & Cary 610 spectrometer (Agilent Technologies Inc., USA) in attenuated total reflectance (ATR) mode. A background signal was recorded with a germanium crystal and the MP was placed on a microscopy slide. Subsequently, three ATR-FTIR spectra spectra (64 runs for each spectrum) in the range $600\,\text{cm}^{-1} \leq \widetilde{\nu} \leq 4000\,\text{cm}^{-1}$ were recorded. The individual spectra were averaged, straightened and corrected for the water vapor and carbon dioxide background.

2.2.3. Optical microscopy

Optical microscope analyses were performed with the VHX-7000 (Keyence Corporation, Japan).

2.2.4. Scanning electron microscopy

For scanning electron microscopy analyses, a GeminiSEM 460 (Carl Zeiss AG, Germany) was operated at an acceleration voltage of 5 kV. For image formation either a secondary electron (SE) or a back-scattered electron (BSE) detector was used. An energy-dispersive X-ray (EDX) analysis system (AZtec v6.0, Oxford Instruments Nanotechnology Tools Limited) was used for elemental analysis of individual MP and to extract elemental distribution maps from recorded data.

2.3. Preparation of pristine MP with different size and morphology

The aim of applying different preparation methods was to produce different particle size fractions with different morphologies. Particle size distributions with mean volume equivalent diameters of $x_{50,3} \in \{3\,\mu\text{m}, 30\,\mu\text{m}, 100\,\mu\text{m}, 300\,\mu\text{m}\}$ were targeted. Different morphologies were obtained by different production processes.

The PSDs of all particle fractions were measured by SLS and are shown in Fig. 1, and the following sections provide details on the production procedures. The particle morphology of selected particles from the individual size fractions was characterized using a scanning electron microscope (SEM) to enable the comparison between particles size fractions of different or similar morphologies. As was discussed in our previous study (Rhein et al., 2022), measuring the zeta potential of the employed MP is challenging: The electrophoretic technique is only suitable for small particles ($\leq 1\,\mu$m), while the streaming potential is only applicable to smooth surfaces like films. However, literature values range from -10 mV to -40 mV for all investigated polymer types and Mag (Rhein et al., 2022) at $pH = 7$.

2.3.1. Polymer types

Polymer powders were purchased from different companies and further processed if required. Table 1 provides an overview of the source and the manufacturing procedure of the polymers used in the experiments.

2.3.2. Cryomilling of MP

The granules of PE, PP, PS, PET and PVCbl were ground to the desired particle diameters in a cryomilling process. The process followed the protocol of the previous work (Rhein et al., 2022; Seghers et al., 2022). For cryomilling, a ball mill (MM400, Retsch GmbH, Germany) was used. $m = 5$g of the polymer granules were loaded into the stainless steel vessel ($V = 35$ mL) together with a stainless steel grinding ball ($d = 20$ mm). The capsule was initially cooled for $t_0 = 10\,min$ in liquid nitrogen ($\vartheta_{N_2(l)} = -196^{\circ}$C) to make the polymers brittle and easier to fragment. The polymers were ground in several cycles. One cycle consisted of grinding for $t_1 = 1\,min$ at $f = 30\,\text{s}^{-1}$ and cooling for $t_2 = 1.5\,min$ in liquid nitrogen. The required number of cycles to achieve the targeted size category depended on the polymer type (see Supplementary Information (SI) Table A.1). The fraction $x_{50,3} = 100\,\mu$m of PP required additional wet sieving, which was carried out by the particle laboratory at the MVM of KIT. Separation with micro-precision sieves in the range of $80\,\mu\text{m} < d < 170\,\mu$m using ethanol as dispersing agent yielded suitable particle size fractions.

2.3.3. Cutting-milling of MP

In addition to the cryomilling process, PVCbl were ground in a cutting mill with turbine function (NanoFract, Germany). Fractions with mean volume equivalent diameters of $x_{50,3} \in \{3\,\mu\text{m}, 30\,\mu\text{m}, 300\,\mu\text{m}\}$ were obtained from NanoFract (Germany). The fraction at $x_{50,3} = 100\,\mu$m was produced by dry sieving of the fraction $x_{50,3} \approx 300\,\mu$m with a separation in the range $80\,\mu\text{m} < d < 170\,\mu$m by the particle laboratory MVM of KIT. The obtained particle size fractions well matched the targeted size ranges (Fig. 1).

2.3.4. Commercially available MP

Additional particle size fractions that were suitable for comparison with the milled MP were acquired commercially and used without processing (Table 1).

2.4. Aging of MP

Two different aging procedures – namely exposure to UV radiation and mechanical (mech) abrasion – were applied to simulate environmental weathering (Sun et al., 2020; Gewert et al., 2015). A third, oxidative (ox) treatment was used to account for frequently applied sample preparation schemes (Philipp et al., 2022; Pfeiffer and Fischer, 2020; Hurley et al., 2018). All aging treatments were investigated individually to avoid potentially additive effects from sequentially

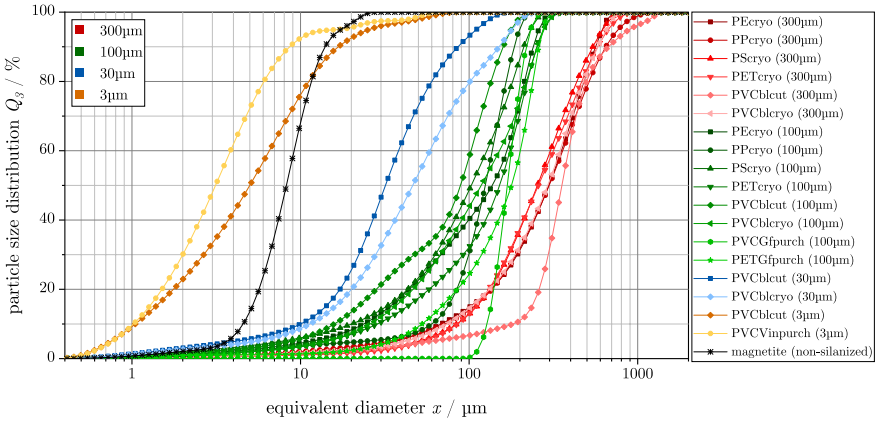

Fig. 1. Particle size distribution of all pristine particle size fractions measured with static laserlight scattering: The different size categories are indicated by color. Different polymer types, manufacturers and preparation procedures yield variations withing each size fraction. Abbreviations: blue (bl), cutting-milled (cut), cryomilled (cryo), Vinnolit (Vin), purchased (purch), Goodfellow (Gf).

Table 1
Overview of the source and the manufacturing procedure of the polymers used in the aging and the magnetic seeded filtration experiments: The polymers were purchased in different shape, either as powders which were used directly in the experiments or as granules which were processed to microplastic particles (MP) by cryomilling (cryo) or cutting-milling (cut) first. Different size fractions between 3 μm and 300 μm were obtained.

Starting material		→	Processed MP system	
Polymer	Manufacturer product	Process	Label	Sizes / µm
PE	Goodfellow ET316305/2	Cryomilling	PEcryo	100, 300
PP	Goodfellow PP306306/1	Cryomilling	PPcryo	100a, 300
PS	Goodfellow ST316311/1	Cryomilling	PScryo	100, 300
PET	Goodfellow ES306313/1	Cryomilling	PETcryo	100, 300
PET	Goodfellow ES306030/2	None	PETGfpurch[b]	100
PVC	fatra NOVODUR	Cryomilling	PVCblcryo[c]	30, 100, 300
PVC	fatra NOVODUR	Cutting-milling	PVCblcut[c]	3, 30, 100[a], 300
PVC	Goodfellow CV316010/4	None	PVCGfpurch[b]	100
PVC	Vinnolit P70	None	PVCVinpurch[b]	3

[a] Required additional fractionation.
[b] MP directly purchased (purch) in powder form from the manufacturer, used without further process.
[c] As PVC from fatra has a different color, it is labeled as blue (bl) to distinguish it from PVC from Goodfellow or Vinnolit.

conducted aging treatments.

2.4.1. UV aging

For UV aging, glass Petri dishes containing $m = 300$ mg of the polymer powders were prepared and covered with 10 μm thin transparent polymer foil to prevent the particles from being blown away by the air cooling system in the weathering chamber (SUNTEST CPS+, Heraeus Holding GmbH, Germany). The samples were irradiated for a duration of $t_{UV} = 500$ h. A xenon lamp with a daylight filter ($300\,nm < \lambda < 800\,nm$) was used, operating at an irradiation power of $P_{Irr} = 700\,W\,m^{-2}$. This approach corresponds to an equivalent aging time of $t_{eq} = 104$ d in the environment, based on the mean global radiation of $P_{DWD} = 140\,W\,m^{-2}, G_{DWD} = 1227 kWhm^{-2}$ measured by Deutscher Wetterdienst in 2022 (Deutscher Wetterdienst, 2022). The temperature during UV aging was kept below $\vartheta \leq 36^{\circ}$C to limit thermal stress. The Petri dishes were shaken at least every two days to allow a uniform irradiation of the MP particles. After the UV exposure, the MP were stored in the dark until use.

2.4.2. Mechanical aging

The mechanical aging process was simulated by adding $m_{MP} = 300$ mg of MP to a glass bottle ($V = 50$ mL) together with $m_{sand} = 10$ g of sand (Krone Feine Gips Quarzsand universal, VG-ORTH GmbH & Co. KG, Germanny). The glass bottles were fixed on the horizontal shaker SM30 (Edmund Bühler GmbH, Germany) and shaken for $t_{mech} = 45$ d at $f = 250\,min^{-1}$. The MP were separated from the sand matrix by density separation in a heavy liquid ($\rho = 1.5\,g\,mL^{-1}$) (Acros Organics $Na_6(H_2W_{12}O_{40})$ * H_2O, Thermo Fisher Scientific Inc., USA). For this purpose, the MP-sand mixture was placed in a centrifuge tube, filled up to $V = 40$ mL with the heavy liquid and dispersed for $t_{sonic} = 2\,min$ in the ultrasonic bath TP 690 A (Bioblock Scientific AG, Switzerland). Subsequently, the dispersion was centrifuged (Rotina 380, Andreas Hettich GmbH + Co. KG, Germany) at $n = 5000\,min^{-1}$, $z/g = 4863$ for $t = 30\,min$. The supernatant with the MP was carefully decanted and centrifuged again, whereas the pellet with sand remained in the tube. After two centrifugation steps, the MP were filtered and dried.

2.4.3. Oxidative aging

The process of oxidative aging was conducted following the protocol of (Philipp et al., 2022), with an extended aging time of $t_{ox} = 24$ h. The oxidative treatment was initiated by putting $m = 300$ mg of the polymer powder into a beaker ($V = 100$ mL) and adding a mixture of H_2O_2 (pure, stabilized, Carl Roth GmbH + Co. KG, Germany, $V_{H_2O_2} = 10$ mL, $c_V = 35\%$), H_2O (arium pro, Sartorius, Germany, $\kappa^{-1} = 18.2$ Mcm, $pH = 5.25$, $V_{H_2O} = 5$ mL), $FeSO_4(FeSO_4{\cdot}7\,H_2O$, for analysis, Merck KGaA, Germany, $V_{FeSO_4} = 1$ mL, $c_n = 2\,mmol\,L^{-1}$) and dihydroxybenzoic acid (3,4-dihydroxybenzoic acid, $\geq 97\%$, Sigma-Aldrich Corporation, USA, $V_{DHBA} = 1$ mL, $c_n = 2\,mmol\,L^{-1}$). The beakers were then covered and shaken at $f = 100\,min^{-1}$ on the horizontal shaker Unimax 1010/Incubator 1000 (Heidolph Instruments GmbH + Co. KG, Germany). After $t_0 = 1$ h, the temperature of the incubator containing the horizontal shaker was set to ($\vartheta_{ox} = 40^{\circ}$C) and kept at this temperature for $t_{ox} = 24$ h. The MP were recovered from the liquid by vacuum filtration onto a polycarbonate filter (Whatman Nuclepore track-etched Polycarbonate, 47 mm, 0.4 μm, GE HealthCare Inc., USA) and rinsed with ultrapure water. Following the filtration, the particles were dried at $\vartheta_{dry} = 40^{\circ}$C for $t_{dry} \geq 12$ h and stored in the dark until use.

2.5. Systematic overview of all MP systems

The particle fractions are referred to by their assigned size category, rather than by their mean diameters for the remainder of this work. Table 2 provides an overview of all the MP size fractions used in this work and shows which aging methods were applied for which size fractions.

2.6. Silanization of magnetite

The initially hydrophilic magnetic particles (Mag, Magnetit extra fein, Kremer Pigmente GmbH + Co. KG, Germany) consisted of magnetite (Fe_3O_4). They have a mean volume equivalent diameter of $x_{50,3} = 7.2\,\mu m$ and their PSD, as measured by SLS is shown in Fig. 1. To trigger the formation of hetero-agglomerates with MP through hydrophobic interactions, they were made hydrophobic by silanization. The procedure follows the protocol described in (Rhein et al., 2022) developed by (Grbic et al., 2019; Frickel et al., 2010; Ji et al., 2017). Pristine Mag ($m_{Mag} = 8.0\,g$) were added to a 200 mL glass bottle together with EtOH (EMSURE, EtOH for analysis, Merck KGaA, Germany, $V_{EtOH} = 72.0\,mL$), hexadecyltrimethoxysilane ($H_3C(CH_2)_{15}Si(OCH_3)_3$, technical, ≥ 85%, Sigma-Aldrich Corporation, USA, $V_{HDTMS} = 1.7\,mL$) and H_3O ($V_{H_2O} = 8.0\,mL$). This suspension was mixed in the overhead shaker Reax 2 (Heidolph Instruments GmbH + Co. KG, Germany) for $t = 24\,h$. The silanized Mag were magnetically separated from the reaction mixture, rinsed three times with EtOH ($V_{EtOH} = 60\,mL$) and dried at $\vartheta_{dry} = 40^{\circ}C$ for $t_{dry} \geq 12\,h$. The hydrophobic Mag were then stored in the dark until use.

The success of the silanization procedure was estimated by analytical particle solvent extraction (APSE) in a previous study (Rhein et al., 2022), following the protocol of (Sygusch and Rudolph, 2021). The fraction of magnetic particles transferred to the non-polar octanol phase increased from 6.5% before silanization to 90% after silanization, demonstrating the efficiency of the process.

2.7. Experimental procedure

The experimental procedure is visualized schematically in Fig. 2 and briefly described below. A more detailed description of the experimental procedure is provided in the SI Chapter B. The initial particle masses $m_{e,MP}$ and $m_{e,Mag}$ were calculated so that the volume ratio between Mag and MP remained constant at $V_{Mag}/V_{MP} = 7.4 \times 10^{-2}$ and that the absolute volume concentrations $c_{V,Mag}$ and $c_{V,MP}$ were comparable to (Rhein et al., 2022). The impact of the volume ratio between Mag and MP was investigated in a previous study (Rhein et al., 2019) and demonstrated an increasing removal efficiency with an increasing Mag to MP ratio. We, therefore, kept this ratio constant, which allowed us to directly relate changes of the removal efficiencies to the (surface) properties of the MP. The calculated polymer (and Mag) masses as well as the calculated concentrations and ratios are given in Table 3. For each individual experiment, the actually weighed masses are listed in the SI Table I.1.

Table 2
Overview of all microplastic particles (MP) systems used in the magnetic seeded filtration experiments: Each cell of the matrix represents a MP fraction of a certain size and a certain polymer type. Each cell/fraction has been divided into sub samples which underwent different aging processes. The available sub samples in each fraction are indicated by pristine (pris), oxidative (ox), ultraviolet (UV) and mechanical (mech) aging. The ✓ symbol marks cells for which all aging methods were available.

MP system	3 μm	30 μm	100 μm	300 μm
PEcryo			✓	✓
PPcryo			pris[a]	✓
PScryo			✓	✓
PETcryo			✓	✓
PVCblcryo		✓	✓	
PVCblcut	pris, ox, UV [b]	✓	pris[a]	✓
PVCpurch	pris, ox, UV [b]			
PVCpurch			✓	
PETpurch			✓	

✓ particles of all different aging methods and pristine ones available.
[a] Required fractionation that made aging impossible due to time constraints.
[b] Significant losses during mechanical aging.

The required amounts of Mag and MP were added to an aqueous solution ($V_{Agg} = 40\,mL$, constant ionic strength of $I = 0.01\,mol\,L^{-1}$, $pH = 7.05$) and dispersed in an ultrasound bath (TP 690 A, Bioblock Scientific AG, Switzerland) for $t_{sonic} = 2min$. The suspension was then put on a horizontal shaker (Unimax 1010, Heidolph Instruments GmbH + Co. KG, Germany) at $f = 180\,min^{-1}$ for $t_{Agg} = 10\,min$ to trigger the formation of hetero-agglomerates. During the mechanical aging experiments, no temperature increase was noticed. We, thus, assume that the temperature remained constant throughout all experiments and did not affect the agglomeration behavior. The hetero-agglomerates were separated from the suspension by placing a permanent magnet next to the glass bottle for $t_{sep} = 2\,min$. After carefully transferring the supernatant into a glass beaker, the bottle was slowly refilled with another $V_{Agg} = 40\,mL$ of the aqueous agglomeration solution and the magnetic separation procedure was repeated to remove remaining non-magnetic agglomerates from the residue. The resulting supernatant was added to the supernatant from the first separation run. The combined supernatant was vacuum filtered on polycarbonate membranes (Whatman Nuclepore track-etched polycarbonate, 47 mm, 0.4 μm, GE HealthCare Inc., USA). Both the polycarbonate membrane containing the particles of the supernatants and the glass bottle with the residual particles were dried at $\vartheta_{dry} = 40^{\circ}C$ for $t_{dry} \geq 12\,h$ and then weighted (AX205 Delta Range, Mettler Toledo Inc., USA). The weighted masses of the particles of the filtered supernatants m_{sup} and of the residues m_{res} were used to calculate the separation efficiency. The mass balance was closed by comparing all weights before and after the experiments, allowing also for the quantification of total mass lost m_{loss} during the experimental procedure. All experiments were conducted in triplicate.

2.8. Determination of the separation efficiency

The separation efficiency A describes the fraction of the magnetically separated MP mass $m_{MP,res}$ relative to the initially added mass $m_{e,MP}$. Assuming a complete recovery of all particles, A_{ideal} can be calculated from the mass of MP in the supernatant $m_{MP,sup}$ according to

$$A_{ideal} = \frac{m_{MP,res}}{m_{e,MP}} = \frac{m_{e,MP} - m_{MP,sup}}{m_{e,MP}} = 1 - \frac{m_{MP,sup}}{m_{e,MP}} \quad . \tag{1}$$

The mass of MP in the supernatant ($m_{MP,sup}$) was corrected to account for the loss of particles during the sample preparation and handling procedures based on the following assumptions. All assumptions were derived from and validated by the results of initial separation experiments described in SI Chapter D.

(i) The total mass lost m_{loss} obtained from the mass balance calculations can be attributed to a loss of Mag and a loss of MPs. The distribution is assumed to be identical to preliminary experiments performed with only MP or Mag resulting in a fraction of MP of $a_{MP} = \frac{m_{MP,loss}}{m_{loss}} = 0.57$.

(ii) The mass of MP lost $m_{MP,loss}$ can be distributed between the mass of MP lost in the supernatant and the loss of MP in the separated fraction. The ratio between these two fractions corresponds to the separation efficiency. The corrected mass $m^{*}_{MP,sup} = m_{MP,sup} + m_{MP,loss}\frac{m_{MP,sup}}{m_{e,MP}}$ accounts for this loss.

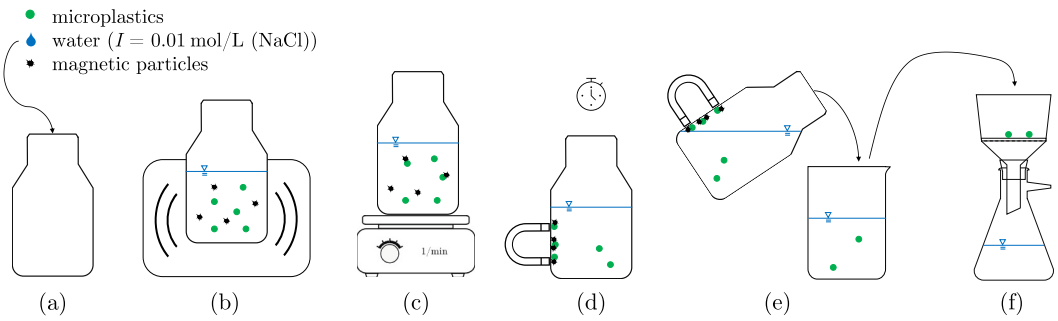

Fig. 2. Schematic of the magnetic seeded filtration (MSF) experiment: a: adding required compounds to reaction bottle, b: dispersing, c: agglomeration, d: magnetic separation, e: decanting, f: filtration and drying.

Table 3
Left: Polymer-specific density and calculated masses $m_{e,MP}$ and concentrations used for initiating agglomeration experiments. Right: Additional system properties used to calculate required experimental MP masses. Calculations are based on a constant volume ratio of microplastic particles (MP) to magnetic particles (Mag) and volume concentrations of 0.039 vol%, in alignment with (Rhein et al., 2022). Abbreviations: Concentration (conc.), blue (bl), purchased (purch), suspension (susp.)

Polymer	Density $\rho_{MP}/\frac{kg}{m^3}$	Conc. $c_{m,MP}/\frac{mg}{mL}$	Mass $m_{e,MP}/mg$
PE	920[a]	0.359	14.35
PP	900[a]	0.351	14.03
PS	1050[a]	0.409	16.37
PET	1380[a]	0.538	21.52
PVCbl	1450[b]	0.565	22.61
PVCpurch[c]	1400[a]	0.546	21.83
PETpurch	1350[a]	0.526	21.05

Susp. volume	V_{Agg}/mL	40
Volume ratio	$\frac{V_{Mag}}{V_{MP}}/-$	7.40×10^{-2}
Conc. MP	$c_{V,MP}/-$	3.90×10^{-4}
Conc. Mag	$c_{V,Mag}/-$	2.88×10^{-5}
	$c_{m,Mag}/\frac{mg}{mL}$	0.150
Density Mag	$\rho_{Mag}/\frac{kg}{m^3}$	5200
Mass Mag	$m_{e,Mag}/mg$	6.00

[a] datasheet of manufacturer.
[b] displacement experiment.
[c] Goodfellow and Vinnolit.

(iii) Mag was completely removed during the magnetic separation and therefore the mass of the supernatant solely consisted of MP: $m_{MP,sup} = m_{sup}$.

Based on these assumptions, the corrected separation efficiency A_{corr} was calculated according to Eq. 2 and referred to as A for the remainder of this work.

$$A := A_{corr} = 1 - \frac{m^*_{MP,sup}}{m_{e,MP}} = 1 - \frac{m_{sup} + a_{MP}\, m_{loss}\, \frac{m_{sup}}{m_{e,MP}}}{m_{e,MP}} \quad (2)$$

3. Results & discussion

The separation efficiency A of MP varied considerably depending on the polymer type, aging process, particle size category and manufacturing method (morphology). An overview of the experimental results is given in Fig. 3 and the influence of each parameter on the separation efficiency is discussed in more detail in the following sections.

3.1. Influence of polymer type on the separation behavior

Separation efficiencies of $A > 80\%$ were obtained for pristine PE, PP and PS, whereas the separation efficiency for pristine PET was in the range of $A \approx 60\%$, in excellent agreement with our previous study (Rhein et al., 2022).

PVCGfpurch reached a separation efficiency of $A = 68.4\% \pm 16.4\%$, whereas the separation efficiency was $A > 80\%$ for PVCbl. The difference in the separation efficiency most likely reflects different chemical compositions of the materials. The FTIR spectra of PVCGfpurch given in the SI Fig. G.2 perfectly matched the spectra of PVC from the database and this material, thus, represents a pure PVC polymer. However, in the FTIR spectra of PVCbl additional oscillations which were characteristic for PMMA were observed.

The separation efficiencies of the different polymer types correlated with their hydrophobicity, suggesting that hydrophobic interactions governed the agglomeration process. Table 4 lists the contact angles measured in a previous work (Rhein et al., 2022) together with the corresponding contact angle interpretations according to (Butt et al., 2003; Israelachvili, 2011). The order of the polymer's hydrophobicity is consistent with predictions resulting from theoretical models (Foster et al., 2020). The repoted contact angles refer to measurements conducted on films of the same materials from the same manufacturers. Measuring the hydrophobicity of particulate solids is challenging (Sygusch and Rudolph, 2021) and was neither feasible for pristine nor aged MP, as they accumulated in the interface during analytical particle solvent extraction as discussed in (Rhein et al., 2022).

The more hydrophobic polymer types are more efficiently separated compared to the less hydrophobic or more hydrophilic ones. As the hydrophobicity of the particles increases, the attractive hydrophobic interaction and thus the collision efficiency α increases until it reaches it's maximum value at $\alpha = 1$ (see (Rhein et al., 2022)). More stable agglomerates are formed, which are subsequently deposited during magnetic separation resulting in a higher separation efficiency. The more hydrophilic properties of PET and PVC may be related to the electronegative oxygen and chlorine atoms present in the structure of these polymers. These form polar groups and allow the formation of hydrogen bonds with surrounding water molecules as shown in SI Fig. E.1. Due to the hydrophobic hydrocarbon backbone, the separation efficiency remains comparatively high at $A > 50\%$ despite the polar functional groups. PE, PP and PS do not have polar groups, are therefore more hydrophobic and separated to a higher extent.

3.2. Influence of particle size on the separation efficiency

Pristine MPs from both size fractions $x_{50,3} \approx 100\,\mu m$ and $x_{50,3} \approx 300\,\mu m$, which were available for all polymer types, showed the same separation efficiency. The production of smaller MP by cryomilling

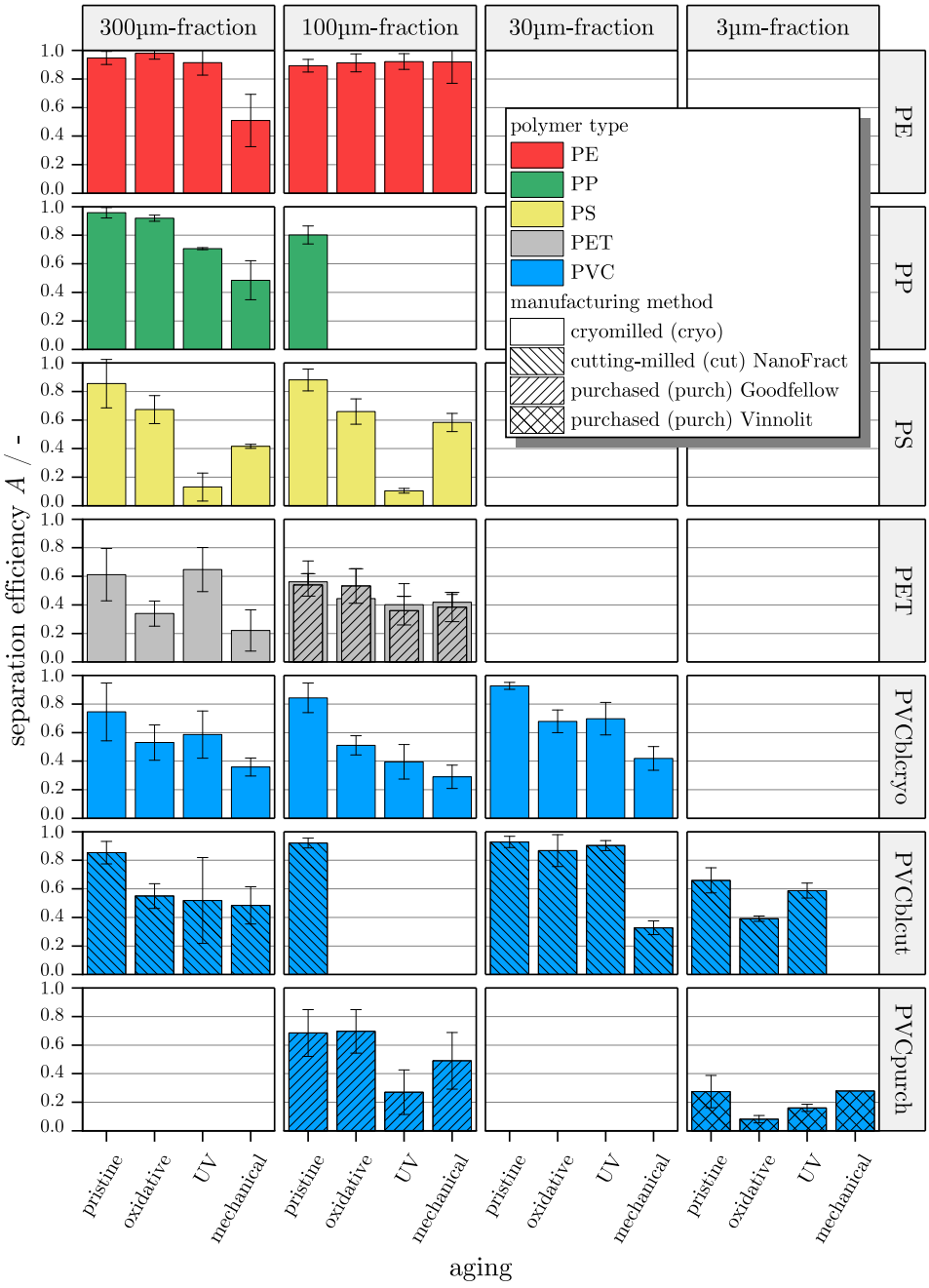

Fig. 3. Separation efficiency A of MP by MSF. The results are structured in a grid according to the design of this study. The polymer type is distinguished by color and row and the columns correspond to the particle size categories. The manufacturing method is indicated by hatching. Each subplot visualizes the influence of the investigated aging mechanisms.

Table 4
Assessment of the polymer's hydrophobicity based on their contact angle (Rhein et al., 2022; Butt et al., 2003; Israelachvili, 2011; Foster et al., 2020).

PP	PE	PS	PVC	PET
$100^\circ \pm 3.4^\circ$	$97^\circ \pm 0.6^\circ$	$90^\circ \pm 3.2^\circ$	$85^\circ \pm 1.3^\circ$	$77^\circ \pm 0.7^\circ$
non-wettening ($\Phi > 90^\circ$)			partially wettening ($\Phi < 90^\circ$)	
← hydrophobic				hydrophilic →

was only possible for PVCbl. Additionally, a fraction $x_{50,3} \approx 3\,\mu$m was provided by NanoFract. The separation efficiency for cryomilled blue PVC in the size range $30\,\mu\text{m} \leq x_{50,3} \leq 300\,\mu$m remained at around $A(\text{PVCblcryo}) \approx 80\%$, with a slightly, although statistically not significant trend of increasing separation efficiency with decreasing particle diameter. The cutting-milled particles were separated with an efficiency of $A(\text{PVCblcut}) \approx 90\%$ and also remained constant in the size range $30\,\mu\text{m} \leq x_{50,3} \leq 300\,\mu$m. However, the separation efficiency for the fraction $x_{50,3} \approx 3\,\mu$m, was significantly lower at $A(3\,\mu\text{m}) = 65.9\% \pm 8.8\%$.

According to (Israelachvili, 2011; Elimelech, 1998), the hydrophobic interaction is proportional to $E_{\text{hyph}} \propto (r_1 + r_2)$ and the electrostatic interaction is proportional to $E_{\text{el}} \propto r_1 r_2/(r_1 + r_2)$. Comparing these proportionalities in Eq. 3 suggests that the hydrophobic interactions are dominant for particles of different diameters ($r_1 \gg r_2$), whereas both interactions are relevant for particles having similar sizes ($r_1 = r_2$). As Mag have a mean particle diameter of $x_{50,3} \approx 8\,\mu$m, the relative

importance of the repulsive electrostatic interaction increased with decreasing particle diameter of MP.

$$\frac{E_{\text{hyph}}}{E_{\text{el}}} = \frac{(r_1 + r_2)^2}{r_1 r_2} = \begin{cases} 4 & , r_1 = r_2 \\ \frac{r_1}{r_2} \gg 1 & , r_1 \gg r_2 \end{cases} \quad (3)$$

To verify this hypothesis, separation experiments with $x_{50,3} \approx 3\,\mu$m MP at different ionic strengths were conducted. The results show that the separation efficiency of particles in this size range increased with increasing ionic strength (Fig. 4). Such an impact of the ionic strength on the separation efficiency was not observed for larger particles MP $x_{50,3} > 100\,\mu$m in previous studies (Rhein et al., 2022). These findings support the hypothesis of increased relevance of electrostatic interactions with decreasing particle diameters, as an increased ionic strength results in the compression of the electric double layer, a reduced range of electrostatic repulsion and, thus, enhanced separation efficiencies (Elimelech, 1998). Our findings are in excellent agreement with results from previous studies (Rhein et al., 2019; Rhein et al., 2023b), where the agglomeration behavior of equally sized magnetic and nonmagnetic particles in the lower μm-range was strongly affected by the ionic strength.

Consequently, the formation of agglomerates depends on the particle size in the following way: For particles of different sizes, i.e. here MP with $d \gtrsim 100\,\mu$m and Mag of 8 μm, attractive hydrophobic interactions are dominant, whereas repulsive electrostatic interactions become relevant for equally sized particles, i.e. here MP with $d \lesssim 10\,\mu$m. This behavior is only relevant if the particles carry a surface charge, which is modulated by the *pH*. Hence, the separation of smaller MP is depending on the ionic strength, the *pH*, and on the size of the magnetic particles.

3.3. Influence of surface morphology on the separation behavior

The morphology of the particles PVCblcut and PVCblcryo, made of the same polymer, differ significantly depending on the milling process (Fig. 5). Additional images recorded with the optical microscope and with an SEM are given in the SI Fig. F.1.

The cryomilled particles reminded of rock fragments, splinters or shreds and the cutting-milled particles were roundish and potato-shaped. Despite these differences, the observed separation efficiencies for the cryo- and cutting-milled, (pristine) MP between 30 μm $\leq x_{50,3} \leq$ 300 μm were similar (Fig. 3). Similarly, the morphology of the powder purchased from Goodfellow and of the cryomilled MP differ substantially as shown in SI Fig. F.2. The cryomilled particles were platelet- and splinter-shaped, whereas the purchased powder were roundish, drop- or rock-shaped. Again, similar separation efficiency were observed for both types of morphologies. Hence, the particle morphology only had a negligible impact on the separation behavior during MSF under the given conditions. A more quantitative analysis of morphology and surface roughness, e.g. via atomic force microscopy, is challenging due to the spherical nature and the small size of the investigated particles. Thus, and considering the negligible impact of morphological differences on the separation efficiency, a further quantification of surface parameters was not pursued.

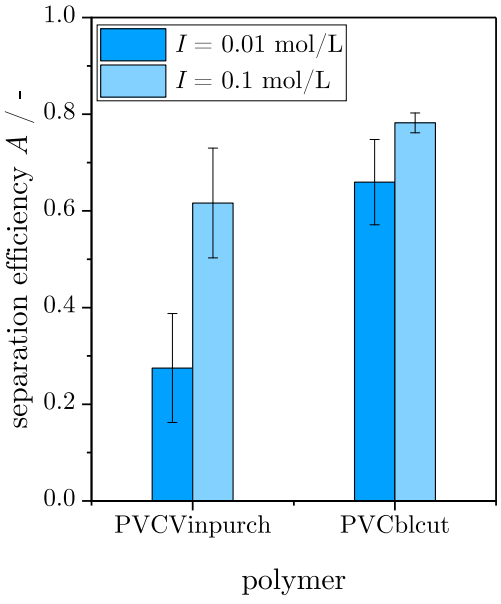

Fig. 4. Separation efficiency of small PVC particles ($x_{50,3} \approx 3\,\mu$m) at different ionic strengths *I*: The increased ionic strength leads to a higher separation efficiency in the lower micron range. Abbreviations: Vinnolit (Vin), purchased (purch), blue (bl), cutting-milled (cut).

3.4. Polymer-specific aging effects on the separation behavior

In this section, the impact of different aging processes on the observed separation efficiency is discussed for the individual polymer types. As already discussed in section 3.1, measuring the hydrophobicity of polymer particles after aging was not possible. Nevertheless, the observed changes in the separation efficiency are related to specific features observed in the FTIR spectra recorded on the aged MPs given in the SI.

3.4.1. Polyethylene

The separation efficiency of the differently aged PE MP remained mostly around $A \approx 90\%$. However, the size fraction $x_{50,3} \approx 300\,\mu$m, showed a strong reduction of separation efficiency due to mechanical aging from $A(\text{pris}) = 94.7\% \pm 4.6\%$ to $A(\text{mech}) = 50.9\% \pm 18.3\%$. The lower separation efficiency correlated with the appearance of a new peak in the FTIR spectrum of the polymer particles at a wavenumber of $\tilde{\nu}_{\text{mech}} = 1032\,\text{cm}^{-1}$ shown in the SI Fig. G.1(a).

3.4.2. Polypropylene

For PP, only aging data in the size category $x_{50,3} \approx 300\,\mu$m are available. Unlike PE, UV-exposure of the PP particles resulted in a decreased separation efficiency from $A(\text{pris}) = 95.7\% \pm 3.7\%$ to $A(\text{UV}) = 70.6\% \pm 0.7\%$. Mechanical aging further lowered the separation efficiency to $A(\text{mech}) = 48.5\% \pm 13.6\%$. Both aging procedures were accompanied by the appearance of new peaks in the FTIR spectra (SI Fig. G.1(b)). Similar to PE, Mechanical aging produced a peak at $\tilde{\nu}_{\text{mech}} = 1032\,\text{cm}^{-1}$ in the FTIR spectrum. UV-irradiation resulted in the formation of a new peak at $\tilde{\nu}_{\text{UV}} = 1730\,\text{cm}^{-1}$, which was absent for PE.

3.4.3. Polystyrene

All aging processes compromised the separation efficiency of PS in both size categories, with very similar trends. The exposure to UV-light resulted in the most pronounced reduction of the separation efficiency, which dropped from $A(\text{pris}) \approx 90\%$ in both size fractions to $A(\text{UV}) < 14\%$. Oxidative aging reduced the separation efficiency to $A(\text{ox}) \approx 70\%$. Mechanical aging resulted in a similar decrease of the separation efficiency to $A(\text{mech}) \in \{58.3\%;\ 41.6\%\}$. Similar to PP, distinct peaks appeared in the FTIR spectrum after mechanical and UV aging (SI Fig. G.1(c)).

3.4.4. Polyethylene terephthalate

The separation efficiency of the pristine PET only reached about $A(\text{pris}) \approx 55\%$ and remained similar after the UV exposure. For the $x_{50,3} \approx 300\,\mu$m size category, the separation efficiency was further reduced after the oxidative and the mechanical treatments to around $A(\text{ox}) \approx 30\%$ and $A(\text{mech}) \approx 20\%$ respectively. A slight - although statistically not significant - reduction of the separation efficiency was also observed for the $x_{50,3} \approx 100\,\mu$m size category.

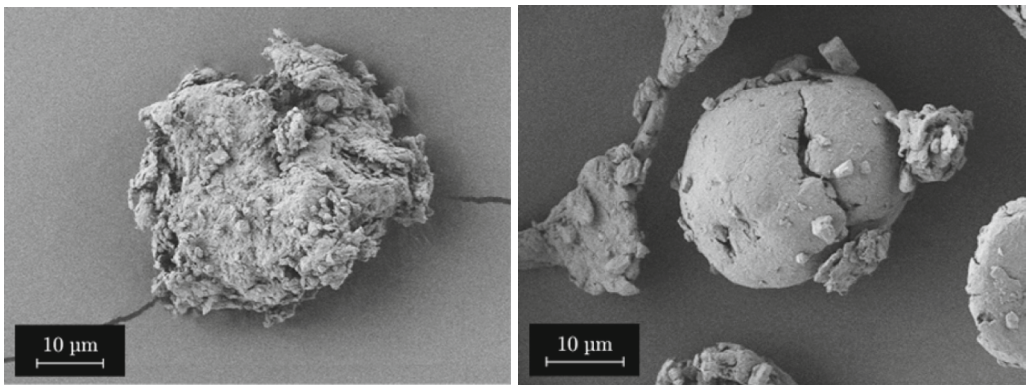

(a) cryomilled blue PVC (b) cutting-milled blue PVC

Fig. 5. Scanning electron microscope images of the blue PVC particles with $x_{50,3} \approx 30\,\mu m$ from different manufacturing processes: The cryomilled PVC particles remind of rocks, splinters or shreds and the cutting-milled particles are more roundish, potato-shaped. Additional images are provided in SI Fig. F.1.

3.4.5. Blue polyvinyl chloride

As discussed in section 3.1, PVCbl likely contains substantial amounts of polymethylmethacrylate (PMMA) and is therefore discussed separately. The separation efficiency of the cryomilled PVCblcryo was reduced after all aging processes and in all size categories, with the mechanical treatment always showing the most pronounced effects. After mechanical aging, the separation efficiencies were between $30\% \lesssim A(\text{mech}) \lesssim 40\%$ for all size categories. Similarly, the separation efficiency of the cryomilled PVCblcryo particles was reduced to $30\% \lesssim A(\text{mech}) \lesssim 50\%$ by mechanical aging. Again, the FTIR spectrum (SI Fig. G.1(e)) shows an additional peak after mechanical aging. The spectrum of the oxidative aged PVCbl remained similar to the spectrum of the pristine material. A possible formation of a UV induced peak at around $\widetilde{\nu}_{UV} = 1730\,cm^{-1}$ may, however, be masked as the spectrum of the pristine materials already showed oscillations in this spectral range.

3.4.6. Polyvinyl chloride (purchased)

The purchased PVC in the size category $x_{50,3} \approx 3\,\mu m$ (from Vinnolit) was only separated to a limited extent. Although oxidative and UV aging further decreased the separation efficiency, the reductions were statistically not significant. Purchased PVC in the size category $x_{50,3} \approx 100\,\mu m$ (from Goodfellow) reached a separation efficiency in the pristine state of $A(\text{pris}) = 68.4\% \pm 16.4\%$, which remained similar after oxidative aging. Analogously to PS, UV irradiation resulted in the most pronounced reduction of the separation efficiency and decreased to $A(\text{UV}) = 27.0\% \pm 15.6\%$. This decrease was accompanied by the appearance of a peak at $\widetilde{\nu}_{UV} = 1730\,cm^{-1}$ in the FTIR spectrum (SI Fig. G.1(g)). Mechanical aging also slightly reduced the mean separation efficiency, although this effect was statistically not significant. The appearance of a peak in the FTIR spectrum after mechanical aging at $\widetilde{\nu}_{mech} = 1032\,cm^{-1}$, may have been masked by overlapping vibrations of the pristine PVC in the range of $\widetilde{\nu} \approx 1000\,cm^{-1}$.

3.5. Discussion on aging mechanisms

3.5.1. Oxidative aging

The separation efficiencies of PS, PET, PVCbl were moderately reduced after the oxidative aging. This treatment was expected to produce hydrophilic hydroxyl groups, reducing the hydrophobic interactions and thus the separation efficiency. The observed reduction of the separation efficiency for PS and PET may be due to hydroxylation at the phenyl(ene) group. During agglomeration, the generated hydroxyl groups were able to form hydrogen bonds to the surrounding water molecules rendering the particle surface more hydrophilic and, thereby, reducing the separation efficiency. However, the effect on the separation efficiency was considerably less compared to the changes caused by UV exposure or mechanical aging. These findings are consistent with results from FTIR measurements, where the spectral features remained unaffected by the oxidative treatment (Philipp et al., 2022). Further, they are in agreement with our previous study (Rhein et al., 2022), where oxidative treatment did not significantly affect the separation behavior.

3.5.2. UV aging

The effects of UV irradiation on the separation efficiency strongly depended on the polymer type. The separation efficiency of PE and PET remained mostly unaffected, but significant reductions were observed for PP, PS and to some extent also for PVC. The change was most pronounced for PS, which was hardly separated at all after UV aging. UV irradiation sets off a radical chain reaction that causes photooxidation of the polymers. In this process, the polymer molecules react with the atmospheric oxygen and form carbonyl groups, which are detected by FTIR spectroscopy as a peak in the spectral range of $\widetilde{\nu} \in \left[1715\,cm^{-1}, 1745\,cm^{-1}\right]$ (Socrates, 1997; Rabek and Rånby, 1974; Yousif and Haddad, 2013). The polar carbonyl groups are able to develop dipole-dipole interactions with the surrounding water molecules. As a consequence, the particles become more hydrophilic, reducing both the strength of the hydrophobic interaction and the separation efficiency. PS was most susceptible to UV radiation due to the aromatic ring (see SI Fig. E.1(e)) which absorbs the UV light.

3.5.3. Mechanical aging

Aging the MP in the sand bed caused a decrease in separation efficiency for almost all polymer types. Only in a few cases, values of $A(\text{mech}) > 50\%$ were achieved. It is remarkable that this change occurred independently of the polymer type and size category and that the separation efficiency – no matter how high $A(\text{pris})$ was – mostly settled in the range of $40\% \lesssim A(\text{mech}) \lesssim 50\%$.

Optical microscope and SEM images (SI Fig. F.3) confirmed that the particle size and shape were largely preserved during the mechanical aging. This is supported by similar particle size distributions, measured before and after the mechanical aging experiments shown in SI Fig. H.1. Additionally, results presented in sections 3.2 and 3.3 showed only limited impacts of the size and the morphology on the separation efficiencies. Therefore, the observed changes in the separation efficiency are unlikely to be related to variations in the size or the morphology of the MPs.

In the FTIR spectra of all polymer types except PET, a peak in the spectral range of $\widetilde{\nu} \in \left[1030\,cm^{-1}, 1100\,cm^{-1}\right]$ appeared after mechanical aging (SI Fig. G.1). This peak reflects oscillations caused by silica, i.e. sand, which may have accumulated on the particle surface during mechanical aging (Socrates, 1997; Grumezescu et al., 2014; Tran et al., 2013). Additional SEM images and elemental distribution maps

indicated that the MP were indeed coated with silica particles (Fig. 6). The BSE images of the mechanically aged PS particles appeared very patchy (Fig. 6a), with the brighter areas reflecting heavier elements, i.e., of silica (Si) and oxygen (O) compared to carbon (C), as confirmed by elemental distribution maps and corresponding elemental spectra (Fig. 6b). The BSE images of the mechanically aged PET particles also showed individual bright spots, (Fig. 6c) which were again associated with Si and O and, thus, reflecting silica particles (Fig. 6d). The silica particles were more evenly distributed on the surface of the PET particles as compared to the PS particles, which most likely resulted from different surface properties of the two MP particle types.

The detection of silica particles on the surfaces of mechanically aged particles explains the reduced separation efficiency. Silica particles are generally hydrophilic (Muster et al., 2001) and thus render the surface of the pristine polymers less hydrophobic, which lowered the separation efficiency.

The aging experiments were all conducted individually which allowed us to identify aging specific changes of the polymer properties. In an environmental setting, a sequential combination of the different aging processes will likely occur and individual aging processes may affect each other in a additive manner. For example, changes of the surface properties of the polymers by UV light may affect how the silicate / sand particles are distributed on the surface of the polymers after mechanical aging. Addressing the importance of such additive effects would, however, require another experimental setup where polymer particles are sequentially aged. In this study, abiotic aging mechanisms were investigated. Biodegradation (biotic aging) relates to specific enzymes that can cleave the polymer backbones, and thus cut the polymer chains into smaller units that can be assimilated by the organisms (enzymatic depolymerization). Such processes, in general, result in more hydrophilic surfaces that would generally lower the MSF efficiency. However, most of the conventional polymers, such as PE, PP and PS are not or only poorly biodegradable in the environment within a reasonable time frame and are thus unlikely to result in surface modifications of the MPs. Nevertheless, over time and depending on the specific environment, these conventional (non-biodegradable) polymers will become coated with an organic layer, a so-called eco-corona. Importance substances include humic acid, fulvic acid, extracellular polymeric substances and proteins, collectively referred to as dissolved organic matter. As demonstrated by Schefer (Schefer et al., 2023), sorption of dissolved organic matter to the MPs tended to decrease the water contact angle and thus resulting in surfaces more hydrophilic surfaces. Thus, we expect that both, initial biodegradation and the formation of an eco-corona will generally lower the separation efficiencies of MPs from aqueous suspensions.

The time scale for our aging experiments correspond to 500 h of UV

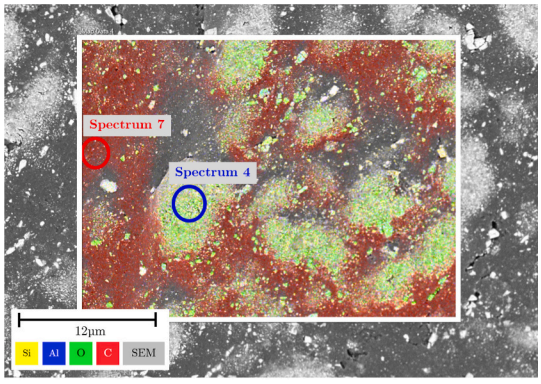

(a) Elemental distribution maps (silicon, aluminum, oxygen, carbon) overlaid on a back-scattered electron image of PS after mechanical aging

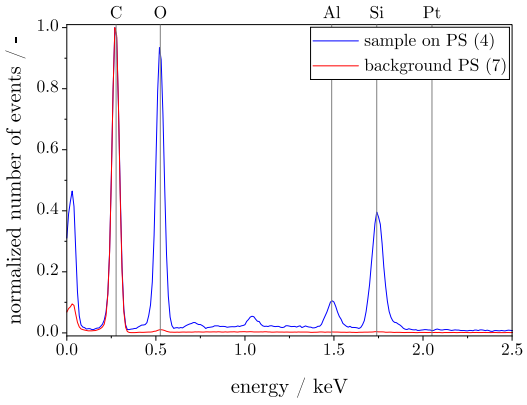

(b) Elemental spectra extracted from the marked areas on PS

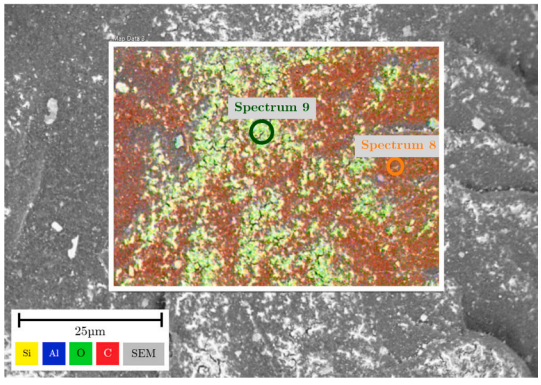

(c) Elemental distribution maps (silicon, aluminum, oxygen, carbon) overlaid on a back-scattered electron image of PET after mechanical aging

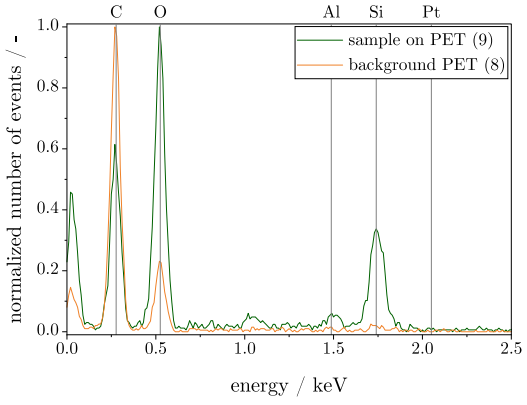

(d) Elemental spectra extracted from the marked areas on PET

Fig. 6. Energy-dispersive X-ray (EDX) elemental analysis of the surface of mechanically aged microplastic particles (MP) of the size fraction $x_{50,3} \approx 300\,\mu m$: The back-scattered electron images show particular deposits on the MP surfaces which according to the EDX spectra are mainly composed of silicon, aluminum and oxygen. The elemental composition indicates that the deposits represent residues of sand.

exposure and 45 days of (intensive) mechanical aging. These experimental aging times translate into roughly 100 days of UV aging in the environment and most likely several 100 days of mechanical aging, although this conversions is very difficult. Nevertheless, the selected time scales allow assessing changes of the surface properties over the first few months of environmental aging, but ultimately reflect a compromise between technical feasibility and long-term fate of MP in the environment. Our results suggest a general trend towards lower removal efficiencies caused by a shift from hydrophobic (pristine) surfaces towards more hydrophilic surfaces over time. A more fundamental understanding of the underlying rate laws, would, however, require time resolved experiments.

4. Conclusions

The polymer type is considered to play a key role during the MSF process. This study extended on this and systematically addressed the impact of particle size, morphology and aging procedures on the performance of MSF. Both particle size and morphology only had limited effects on the separation efficiency. Nevertheless, our data suggest a transition from hydrophobic- to electrostatic-dominated agglomeration when MP sizes decreased into the single-digit μm-range and thus became similar to the size of Mag. An oxidative treatment, often included as an integral part of analytical procedures, only had negligible impacts on the separation behavior, in line with previous findings. However, environmental weathering dramatically affected MP properties and behavior: Mechanical aging (in a sandy environment) reduced the hydrophobicity and therefore the separation efficiency due to an accumulation of silica particles on the MP surface. Remarkably, this occurs across all polymer types and size fractions. UV-induced aging was more polymer-specific and resulted in the chemical alteration of the MP surface. The influence was most pronounced for PS.

The pathways of MP in the environment are strongly influenced by their surface properties, agglomeration behavior with natural particles and their affinity to water. This study highlights the manifold of possible alterations to the MP surface and the complexity in predicting the environmental behavior of MP systems. It therefore challenges the use of pristine MP as representative model system and raises the need for suitable reference materials that adequately address the specific environmental history of MP. This study indicated that MSF is sensitive towards surface changes resulting from environmental aging of MP and the separation efficiency might, therefore, be used as proxy to assess the agglomeration behavior and hydrophobic properties of (environmentally aged) MP. MSF may, therefore, be further developed into a valuable analytical technique.

CRediT authorship contribution statement

Steffen Kaiser: Writing – review & editing, Writing – original draft, Visualization, Methodology, Investigation, Formal analysis, Data curation, Conceptualization. **Ralf Kaegi:** Writing – review & editing, Writing – original draft, Supervision, Project administration, Methodology, Investigation, Formal analysis, Conceptualization. **Frank Rhein:** Writing – review & editing, Writing – original draft, Supervision, Project administration, Methodology, Conceptualization.

Declaration of competing interest

The authors declare that they have no known competing financial interests or personal relationships that could have appeared to influence the work reported in this paper.

Acknowledgment

The research stay at Eawag resulting in the present work was friendly supported by a cooperation of MVM and Eawag. The company fatra is thanked for providing blue PVC granules and the company NanoFract is thanked for providing different size fractions of the blue PVC material. We thank Brian Sinnet and Matthias Philipp for their support in the lab. The electron microscopy center of Empa is thanked for support during electron microscopy analyses.

Supplementary data

Supplementary data to this article can be found online at https://doi.org/10.1016/j.scitotenv.2024.177353.

Data availability

Data will be made available on request.

References

Andrady, A.L., 2011. Microplastics in the marine environment. Mar. Pollut. Bull. 62 (8), 1596–1605. https://doi.org/10.1016/j.marpolbul.2011.05.030.
Andrady, A.L., 2017. The plastic in microplastics: a review. Mar. Pollut. Bull. 119 (1), 12–22. https://doi.org/10.1016/j.marpolbul.2017.01.082.
Andrady, A.L., Neal, M.A., 2009. Applications and societal benefits of plastics. Philos. Trans. R. Soc. Lond. Ser. B Biol. Sci. 364 (1526), 1977–1984. https://doi.org/10.1098/rstb.2008.0304.
Birch, Q.T., Potter, P.M., Pinto, P.X., Dionysiou, D.D., Al-Abed, S.R., 2020. Sources, transport, measurement and impact of nano and microplastics in urban watersheds. Rev. Environ. Sci. Biotechnol. 19, 275–336. https://doi.org/10.1007/s11157-020-09529-x.
Butt, H.-J., Graf, K., Kappl, M., 2003. Physics and chemistry of interfaces. In: Physics Textbook. Wiley-VCH, Weinheim. https://doi.org/10.1002/3527602313.
Deutscher Wetterdienst, 2022. Global-, Diffus- und Direktstrahlung: Monats- und Jahressummen sowie Abweichungen: Strahlungskarten und Infos (accessed: 04/26/24). URL. https://www.dwd.de/DE/leistungen/solarenergie/strahlungskarten_sum.html#buehneTop.
Elimelech, M., 1998. Particle Deposition and Aggregation: Measurement, Modelling, and Simulation, Colloid and Surface Engineering Series. Butterworth-Heinemann, Oxford and Boston. https://doi.org/10.1016/B978-0-7506-7024-1.X5000-6.
Foster, J.C., Akar, I., Grocott, M.C., Pearce, A.K., Mathers, R.T., O'Reilly, R.K., 2020. The role of hydrophobicity in polymer phenomena: 100th anniversary of macromolecular science viewpoint. ACS Macro Lett. 9 (11), 1700–1707. https://doi.org/10.1021/acsmacrolett.0c00645.
Frickel, N., Messing, R., Gelbrich, T., Schmidt, A.M., 2010. Functional silanes as surface modifying primers for the preparation of highly stable and well-defined magnetic polymer hybrids. Langmuir 26 (4), 2839–2846. https://doi.org/10.1021/la902904f.
Gewert, B., Plassmann, M.M., MacLeod, M., 2015. Pathways for degradation of plastic polymers floating in the marine environment. Environ Sci Process Impacts 17, 1513–1521. https://doi.org/10.1039/C5EM00207A.
Geyer, R., Jambeck, J.R., Law, K.L., 2017. Production, use, and fate of all plastics ever made. Sci. Adv. 3 (7), e1700782. https://doi.org/10.1126/sciadv.1700782.
Grbic, J., Nguyen, B., Guo, E., You, J.B., Sinton, D., Rochman, C.M., 2019. Magnetic extraction of microplastics from environmental samples. Environ. Sci. Technol. Lett. 6 (2), 68–72. https://doi.org/10.1021/acs.estlett.8b00671.
Grumezescu, A.M., Ghitulica, C.D., Voicu, G., Huang, K.-S., Yang, C.-H., Ficai, A., Vasile, B.S., Grumezescu, V., Bleotu, C., Chifiriuc, M.C., 2014. New silica nanostructure for the improved delivery of topical antibiotics used in the treatment of staphylococcal cutaneous infections. Int. J. Pharm. 463 (2), 170–176. https://doi.org/10.1016/j.ijpharm.2013.07.016.
Hurley, R.R., Lusher, A.L., Olsen, M., Nizzetto, L., 2018. Validation of a method for extracting microplastics from complex, organic-rich, environmental matrices. Environ. Sci. Technol. 52 (13), 7409–7417. https://doi.org/10.1021/acs.est.8b01517.
Israelachvili, J.N., 2011. Intermolecular and Surface Forces, 3rd edition. Academic Press, Burlington, MA. https://doi.org/10.1016/C2009-0-21560-1.
Jambeck, J.R., Geyer, R., Wilcox, C., Siegler, T.R., Perryman, M., Andrady, A., Narayan, R., Law, K.L., 2015. Marine pollution: plastic waste inputs from land into the ocean. Science (New York, N.Y.) 347 (6223), 768–771. https://doi.org/10.1126/science.1260352.
Ji, T., Ma, C., Brisbin, L., Mu, L., Robertson, C.G., Dong, Y., Zhu, J., 2017. Organosilane grafted silica: quantitative correlation of microscopic surface characters and macroscopic surface properties. Appl. Surf. Sci. 399, 565–572. https://doi.org/10.1016/j.apsusc.2016.11.241.
Koltzenburg, S., Maskos, M., Nuyken, O., 2014. Polymere: Synthese, Eigenschaften und Anwendungen. Springer, Berlin and Heidelberg. https://doi.org/10.1007/978-3-642-34773-3.
Liebmann, B., 2015. Mikroplastik in der Umwelt: Vorkommen, Nachweis und Handlungsbedarf, report rep-0550 Edition. Umweltbundesamt, Wien.
Muster, T.H., Prestidge, C.A., Hayes, R.A., 2001. Water adsorption kinetics and contact angles of silica particles. Colloids Surf. A Physicochem. Eng. Asp. 176 (2), 253–266. https://doi.org/10.1016/S0927-7757(00)00600-2.
Pfeiffer, F., Fischer, E.K., 2020. Various digestion protocols within microplastic sample processing—evaluating the resistance of different synthetic polymers and the

efficiency of biogenic organic matter destruction. Front. Environ. Sci. 8. https://doi.org/10.3389/fenvs.2020.572424.
Philipp, M., Bucheli, T.D., Kägi, R., 2022. The use of surrogate standards as a qa/qc tool for routine analysis of microplastics in sewage sludge. Sci. Total Environ. 835, 155485. https://doi.org/10.1016/j.scitotenv.2022.155485.
Plastics – the facts 2023 (accessed: 04/26/24) (2023). URL. https://plasticseurope.org/knowledge-hub/plastics-the-fast-facts-2023.
Rabek, J.F., Rånby, B., 1974. Studies on the photooxidation mechanism of polymers. i. Photolysis and photooxidation of polystyrene. J. Polym. Sci., Polym. Chem. Ed. 12 (2), 273–294. https://doi.org/10.1002/pol.1974.170120203.
Rhein, F., Scholl, F., Nirschl, H., 2019. Magnetic seeded filtration for the separation of fine polymer particles from dilute suspensions: microplastics. Chem. Eng. Sci. 207, 1278–1287. https://doi.org/10.1016/j.ces.2019.07.052.
Rhein, F., Kaiser, S., Rhein, M., Nirschl, H., 2021. Agglomerate processing and recycling options in magnetic seeded filtration. Chem. Eng. Sci. 238, 116577. https://doi.org/10.1016/j.ces.2021.116577.
Rhein, F., Nirschl, H., Kägi, R., 2022. Separation of microplastic particles from sewage sludge extracts using magnetic seeded filtration. Water research X 17, 100155. https://doi.org/10.1016/j.wroa.2022.100155.
Rhein, F., Hibbe, L., Nirschl, H., 2023a. Hybrid modeling of hetero-agglomeration processes: a framework for model selection and arrangement. Eng. Comput. https://doi.org/10.1007/s00366-023-01809-8.
Rhein, F., Zhai, O., Schmid, E., Nirschl, H., 2023b. Multidimensional separation by magnetic seeded filtration: experimental studies. Powders 2 (3), 588–606. https://doi.org/10.3390/powders2030037.
Schefer, R.B., Armanious, A., Mitrano, D.M., 2023. Eco-corona formation on plastics: adsorption of dissolved organic matter to pristine and photochemically weathered polymer surfaces. Environ. Sci. Technol. 57 (39), 14707–14716. https://doi.org/10.1021/acs.est.3c04180.
Seghers, J., Stefaniak, E.A., La Spina, R., Cella, C., Mehn, D., Gilliland, D., Held, A., Jacobsson, U., Emteborg, H., 2022. Preparation of a reference material for microplastics in water-evaluation of homogeneity. Anal. Bioanal. Chem. 414 (1), 385–397. https://doi.org/10.1007/s00216-021-03198-7.
Shi, X., Zhang, X., Gao, W., Zhang, Y., He, D., 2022. Removal of microplastics from water by magnetic nano-fe3o4. Sci. Total Environ. 802, 149838. https://doi.org/10.1016/j.scitotenv.2021.149838.
Socrates, G., 1997. Infrared Characteristic Group Frequencies: Tables and Charts, 2nd edition. Wiley, Chichester.
Sun, Y., Yuan, J., Zhou, T., Zhao, Y., Yu, F., Ma, J., 2020. Laboratory simulation of microplastics weathering and its adsorption behaviors in an aqueous environment: a systematic review. Environ. Pollut. 265, 114864. https://doi.org/10.1016/j.envpol.2020.114864.
Sygusch, J., Rudolph, M., 2021. A contribution to wettability and wetting characterisation of ultrafine particles with varying shape and degree of hydrophobization. Appl. Surf. Sci. 566, 150725. https://doi.org/10.1016/j.apsusc.2021.150725.
Thompson, R.C., Olsen, Y., Mitchell, R.P., Davis, A., Rowland, S.J., John, A.W.G., McGonigle, D., Russell, A.E., 2004. Lost at sea: where is all the plastic? Science (New York, N.Y.) 304 (5672), 838. https://doi.org/10.1126/science.1094559.
Tran, T.N., van Anh Pham, T., Phung Le, M.L., Thoa Nguyen, T.P., van Tran, M., 2013. Synthesis of amorphous silica and sulfonic acid functionalized silica used as reinforced phase for polymer electrolyte membrane. Adv. Nat. Sci. Nanosci. Nanotechnol. 4 (4), 045007. https://doi.org/10.1088/2043-6262/4/4/045007.
Yousif, E., Haddad, R., 2013. Photodegradation and photostabilization of polymers, especially polystyrene: review. SpringerPlus 2, 398. https://doi.org/10.1186/2193-1801-2-398.
Zhang, Y., Jiang, H., Bian, K., Wang, H., Wang, C., 2021a. A critical review of control and removal strategies for microplastics from aquatic environments. J. Environ. Chem. Eng. 9 (4), 105463. https://doi.org/10.1016/j.jece.2021.105463.
Zhang, Y., Zhao, J., Liu, Z., Tian, S., Lu, J., Mu, R., Yuan, H., 2021b. Coagulation removal of microplastics from wastewater by magnetic magnesium hydroxide and pam. Journal of Water Process Engineering 43, 102250. https://doi.org/10.1016/j.jwpe.2021.102250.